Available online at www.sciencedirect.com
SCIENCE DIRECT®
Journal of Crystal Growth 248 (2003) 50–55
JOURNAL OF CRYSTAL GROWTH
www.elsevier.com/locate/jcrysgro

Growth and p-type doping of ZnSeTe on InP

Matthias Strassburg[a,*], Martin Strassburg[a], O. Schulz[a], U.W. Pohl[a], A. Hoffmann[a], D. Bimberg[a], A.G. Kontos[b], Y.S. Raptis[b]

[a] *Technische Universität Berlin, Institut für Festkörperphysik Sekr. PN 5-2, Hardenbergstr. 36, 10623 Berlin, Germany*
[b] *Faculty of Applied Sciences, National Technical University, 15780 Athens, Greece*

Abstract

Metalorganic vapour phase epitaxy and the p-type doping of ZnSeTe layers on InP (1 0 0) using phosphorus acceptors are presented. The influences of molar ratio in the vapour phase and the ZnCdSe buffer are described. The dependence of the free hole concentration on the P incorporation into ZnSeTe and on the composition of the layers is revealed. The p-type conduction is verified by $C-V$ profiling. Best crystalline quality is found for lattice-matched layers, while highest p-type conductivity is achieved with Te-rich layers. Free hole concentrations of 3×10^{18} and $1\times10^{17}\,\mathrm{cm}^{-3}$ are obtained for strained and lattice matched ZnSeTe layers, respectively.

PACS: 81.05.Dz; 78.55.Et; 73.61.Ga; 81.15.Gh

Keywords: A1. p-Type doping; A3. Metalorganic vapor phase epitaxy; B1. Phosphorus acceptor; B1. ZnSeTe; B2. Semiconducting II–VI materials

1. Introduction

ZnSe and ZnTe show different characteristics in p-type doping, independent of the growth method [1]. Since ZnSe-based structures grown on GaAs substrate by MOCVD cannot be highly p doped to achieve sufficient conductivity, this growth method could not be established as a standard for producing II–VI light emitters. For ZnTe, p-type doping is more successful, although a free hole concentration exceeding $1\times10^{19}\,\mathrm{cm}^{-3}$ was only achieved at a growth temperature as high as 500°C [2]. At a reduced temperature of about 350°C, a free hole concentration of $2\times10^{17}\,\mathrm{cm}^{-3}$ was reported [3]. Application of such contact layers for devices on GaAs are limited by the strong lattice mismatch between ZnTe and GaAs of $\Delta a/a = 7.7\%$.

A change of substrate from GaAs to InP allows lattice match for $ZnSe_{0.50}Te_{0.50}$ layers. Since p-type doping of MBE-grown ternary alloys leads to free hole concentrations of $1\times10^{19}\,\mathrm{cm}^{-3}$ for Te fractions between 0.40 and 1 [4], an improved p-type doping is expected as well for MOCVD growth. In this work, indeed p-type doping of ternary ZnSeTe using MOCVD is demonstrated for the first time. Furthermore, the influence of the composition of $ZnSe_{1-x}Te_x$ and the acceptor concentration on the hole concentration is studied in detail.

*Corresponding author. Tel.: +49-30-314-22182; fax: +49-30-314-22569.
E-mail address: matthias@sol.physik.tu-berlin.de (M. Strassburg).

0022-0248/03/$ - see front matter
PII: S0022-0248(02)01893-6

2. Experimental set-up

Epitaxial layers were grown in a horizontal MOCVD reactor at 380°C and 100 mbar total pressure. We used hydrogen carrier gas, and dimethylcadmium, diisopropyltelluride, dimethylzinc-triethylamine, ditertiarybutylselenide and tertiarybutylphoshine precursors. The growth rate of ZnSeTe was 300 nm/h and about 1 μm/h for the ZnCdSe buffer layers.

X-ray measurements were performed on a Philips Xpert PW3050/65 diffractometer using a germanium (2 2 0) 4 bounce hybrid monochromator with Goebel mirror; $\omega/2\theta$ scans were recorded using a silicon (0 0 4) analyser crystal which reduces the contribution of tilted Bragg planes. Micro-Raman spectra were recorded at room temperature in backscattering geometry with a lateral resolution of 1 μm^2. The Raman signal was analysed by a Jobin–Yvon spectrometer operating in subtractive mode and was detected by a liquid-N_2 cooled CCD camera. Photoluminescence measurements were performed using an He-flow cryostat cooled to 8 K and the 325 nm line of a He–Cd laser for excitation. The emitted light was analysed using a 0.85 m Czerny–Turner double monochromator and a PM tube. The carrier concentration of layers grown on semi-insulating InP was measured by a $C-V$ profiler.

3. Epitaxy of ZnSeTe

Due to the large lattice mismatch between ZnTe [5] and ZnSe [6] and the comparatively smaller lattice constant of GaAs, epitaxy of $ZnSe_{1-x}Te_x$ on GaAs always leads to compressively strained layers. To avoid the strain-driven structural defect formation, the Te fraction must be kept low. Hence, layers and structures with good crystalline quality on GaAs substrate were reported only for a Te fraction of less than 10% [7]. The alternative use of InP substrates allows lattice match and thus strain-free $ZnSe_{1-x}Te_x$ structures with a large Te fraction of $x = 50\%$. The dependence of Te incorporation into $ZnSe_{1-x}Te_x$/InP epilayers on the gas flow ratio is investigated first. $ZnSe_{1-x}Te_x$ layers with a Te fraction ranging between 20% and 95% and a thickness of 300 nm were grown on a 100 nm thick ZnCdSe buffer on InP. The ZnCdSe buffer was found to be crucial. The full-width at half-maximum (FWHM) for $\omega/2\theta$ scans was reduced from more than 300 arcsec for layers without a buffer to below 150 arcsec for layers with at least a 50 nm thick ZnCdSe buffer. For the growth of the ZnSeTe layers, the Se flux was varied while the Zn and the Te fluxes remained constant. A linear rise of the Te fraction is found for decreasing Se flux (inset of Fig. 1). A significant excess of Zn in the gas phase was applied to suppress donor like defects [8].

The excellent crystalline quality of the ZnSeTe/InP epilayers reveals the benefit of epitaxy on InP substrate as compared to epitaxy on GaAs. While $ZnSe_{1-x}Te_x$ layers on GaAs with a Te fraction above 10% have an X-ray FWHM of 1000 arcsec [7], the X-ray FWHM decreases linearly for $ZnSe_{1-x}Te_x$/InP layers when approaching lattice match on InP (Fig. 1). An almost unstrained layer ($\Delta a/a < 0.3\%$) has a $\omega/2\theta$ FWHM of 144 arcsec (Fig. 2). The broader peaks of the $\Delta\omega$ scan display the mosaicity of the crystal as previously found for MOCVD-grown ZnMgCdSe layers [9]. The discrepancy between the simulation and the scan

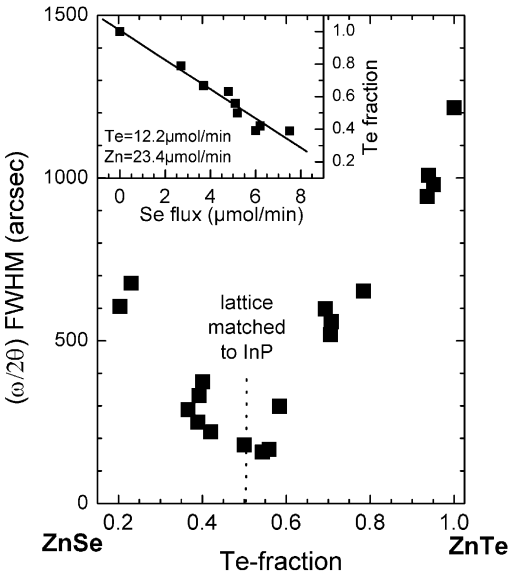

Fig. 1. Dependence of Te incorporation into $ZnSe_{1-x}Te_x$ layers on the gas phase composition (inset) and influence of the composition on the $\omega/2\theta$ X-ray reflection FWHM.

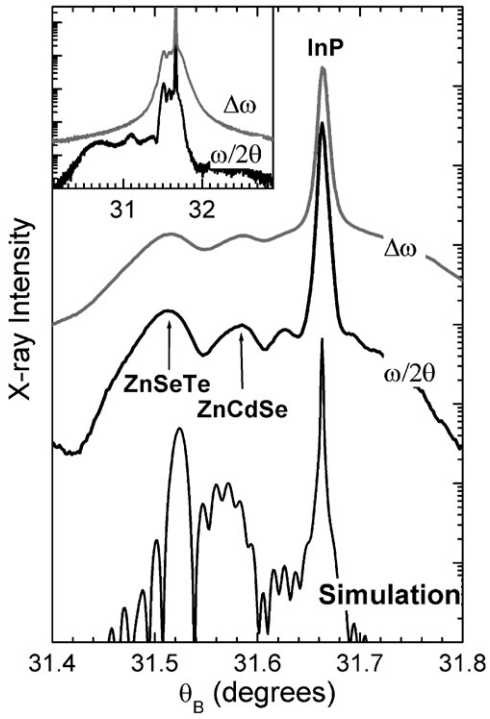

Fig. 2. Comparison between $\omega/2\theta$ and $\Delta\omega$ X-ray spectra for an almost lattice matched alloy of $ZnSe_{0.47}Te_{0.53}$ on a ZnCdSe buffer on InP. The broadening of the $\Delta\omega$ curve shows the mosaic in the layer (for detailed discussion see text). The extended $\omega/2\theta$ scan reveals compositional fluctuations (inset).

originates from partial phase separation. Te-rich phases can be clearly observed in the entire $\omega/2\theta$ scan (inset of Fig. 2).

The homogeneity of the layers was investigated by Raman spectroscopy. A typical spectrum taken with the 514 nm line of an Ar^+ laser for a ZnSeTe layer without a ZnCdSe buffer (sample (a)) is presented in the inset of Fig. 3 and shows the first-order LO and TO Raman peaks as well as the second-order 2LO peak. The spectra comply with the expected one-mode behaviour of the ternary $ZnSe_{1-x}Te_x$ compound [10], according to which one LO and one TO band are observed with frequencies intermediate between those of the binary ZnSe and ZnTe compounds. Since the TO band is poorly resolved, we have used the average $\Omega = (2\omega_{LO} + \omega_{2LO})/4$ for the characterisation of our samples in terms of elemental homogeneity and strains.

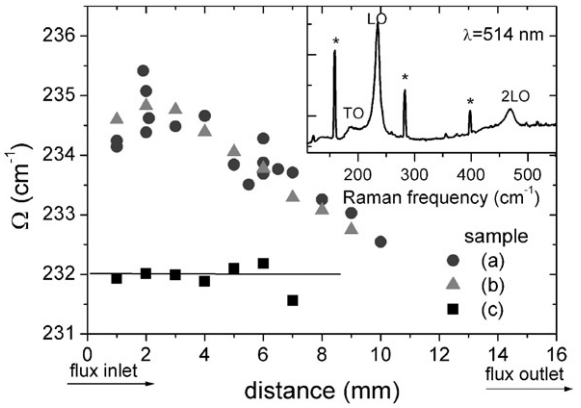

Fig. 3. Raman microanalysis of ZnSeTe layers with differently thick ZnCdSe buffers along the direction inlet to outlet of the precursor flux during growth (for detailed discussion see text). Sample (c) shows no systematic lateral dependence of the Raman frequency. Inset: Characteristic Raman spectrum of sample (a) excited at 514 nm. Peaks marked with stars are emission lines from an Ar lamp used for calibration.

The influence of the ZnCdSe buffer thickness on the homogeneity of the ZnSeTe layer becomes especially evident in Micro-Raman scanning. Such scans with a step width of 1 mm in the direction of the precursor vapour flux are presented for buffer thicknesses of 0 nm (sample (a)), 10 nm (b) and 100 nm (c) (Fig. 3). The approach of Ω for sample (c) to the expected frequency for a lattice matched ZnSeTe epilayer (solid line at $232\,cm^{-1}$) shows that the introduction of a 100 nm ZnCdSe buffer layer improves the quality of the epilayers towards coherent growth. Furthermore, a strong composition change along the scanning direction is clearly observable for samples (a) and (b), where Ω shifts approximately linearly with the distance, with a slope of about $0.25\,cm^{-1}\,mm^{-1}$. This macroscopic compositional variation is the result of a depletion of Se precursors in the gas phase in the flux direction since scanning of sample (b) perpendicular to the flux direction does not show this linear distance dependence. On the other hand, the Raman frequency remains constant over a large area in the centre of the sample (c). This indicates a quite homogeneous elemental composition in this area in agreement with X-ray results.

4. Phosphorus doping of ZnSeTe

Phosphorus is an appropriate acceptor for ZnTe grown by MOCVD at temperatures significantly below 400°C [11]. Using the same growth conditions as for undoped layers, the incorporation of P into $ZnSe_{0.5}Te_{0.5}$ depends linearly on its gas phase supply. Secondary ion mass spectroscopy shows that the linearity exists over the whole investigated range up to $8\times10^{18}\,cm^{-3}$ (Fig. 4). There is no significant broadening of the X-ray reflections ($\omega/2\theta$ curves) due to acceptor incorporation. Phosphorus doping does not lead to a change of the growth rate, but the incorporation efficiency of the group VI elements is affected. The larger the phosphorus supply, the more selenium is found in the solid phase. For a P concentration of $5\times10^{18}\,cm^{-3}$ the Se flux has to be reduced by 35% to maintain the lattice matched composition of the ternary alloy.

4.1. Dependence of the free hole concentration on phosphorus concentration

To prove the conductivity of ZnSeTe:P, 600 nm thick layers of $ZnSe_{0.5}Te_{0.5}$ were grown on ~50 nm thick $Zn_{0.48}Cd_{0.52}Se$ buffers on InP:Fe.

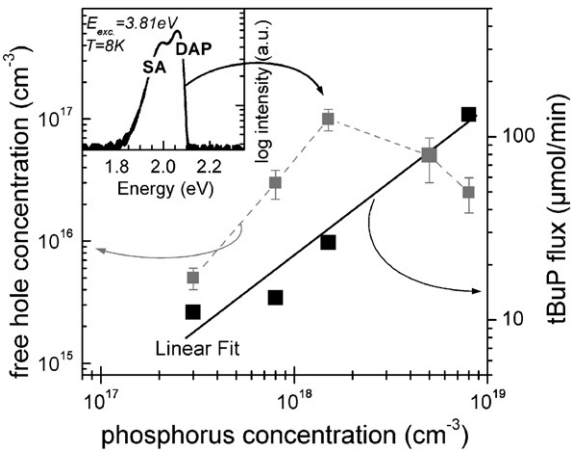

Fig. 4. Dependence of the phosphorus incorporation into $ZnSe_{0.5}Te_{0.5}$ on the tertiarybutylphophine flux in the gas phase (right) and free hole concentration as a function of the phosphorus concentration (left). The PL spectrum of $ZnSe_{0.5}Te_{0.5}$:P (sample (d)) shows the DAP and the SA emission (inset).

The tertiarybutylphosphine flux was varied from 0 to 132 µmol/min corresponding to a P concentration up to $8\times10^{18}\,cm^{-3}$. The free hole concentration $[N_A^- - N_D^+]$ rises up to $1\times10^{17}\,cm^{-3}$ for a P concentration of $1.5\times10^{18}\,cm^{-3}$ (sample (d)) (Fig. 4). Simultaneously, the activation ratio increases up to 7%. Larger P concentrations lead to strong compensation. An analogous reduction of the p-conductivity due to formation of a (V_{Se}–Zn–N_{Se}) defect complex was also observed for MBE-grown ZnSe:N [12–14]. The photoluminescence of moderately P-doped $ZnSe_{0.5}Te_{0.5}$ is dominated by near-bandgap emission, particularly by the donor acceptor pair transition (DAP) at 2.06 eV and the self activated-luminescence (SA) at 1.96 eV (inset Fig. 4).

Since the DAP maximum lies about 100 meV below the band gap for ZnSe and 90 meV for ZnTe, it can be expected to be similar for the ternary alloy. Thus the band gap energy of the ZnSeTe can be calculated to 2.16 eV, close to the value reported for MBE-grown and N-doped layers [4]. Hence the binding energy of the bound exciton, which is 10 meV for both ZnSe:P and ZnTe:P [15,11], can be assumed to be the same for $ZnSe_{0.5}Te_{0.5}$. Such large binding energies imply a deep acceptor and hence a low thermal activation. The band at 1.96 eV is identified as the self-activated luminescence. In ZnSeTe, this luminescence originates from a neutral defect complex formed by a Zn Vacancy, a Se or Te atom and a positively charged donator analogue to ZnSe [14].

4.2. Influence of the Te fraction on the conductivity

Since ZnSe and ZnTe show different characteristics in doping, it is important to investigate their influence on the ternary alloy. Therefore, the Te fraction was varied from $0.20<x<0.75$ for a constant phosphorus concentration of $5\times10^{18}\,cm^{-3}$. The Se-rich compounds ($x<0.40$) show n-type conduction independent of composition. For a Te fraction above 0.46 p-type conductivity occurs. The larger the Te fraction the larger the p-type doping level (Fig. 5). In addition, the compensation decreases with increasing Te fraction. $ZnSe_{0.25}Te_{0.75}$:P has a free hole concentration of $3\times10^{18}\,cm^{-3}$ (sample (e)). This is

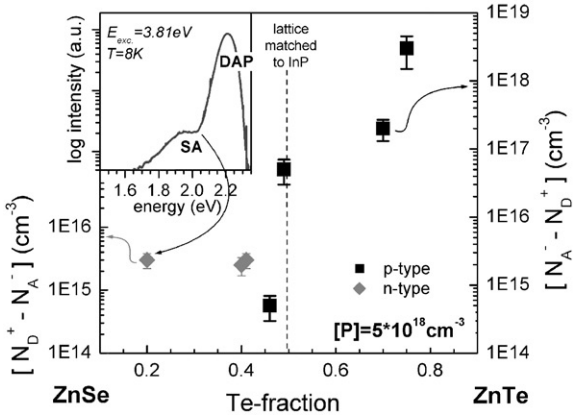

Fig. 5. Free carrier concentration in $ZnSe_{1-x}Te_x$ as a function of the Te fraction; p-type conductivity occurs for a fraction above 0.46. The PL spectrum of $ZnSe_{0.8}Te_{0.2}$ shows the DAP and the SA emission (inset).

the highest p-type doping level ever reported for MOCVD-grown ZnSe or ZnTe grown below 400°C.

It was shown above for undoped layers that the crystalline quality deteriorates with increasing lattice mismatch (Fig. 2). The $\omega/2\theta$ FWHM of layers with a strain $\Delta a/a$ of more than 2% is about three times larger than for lattice matched layers. Because of the large strain, this broadening occurs due to strain-induced defect formation. The effect of the defects on the electrical properties of ZnSeTe:P-layers is shown in the following section.

4.3. Electrical characterisation

With respect to electrical operation of light emitters the mobility of strained and unstrained layers are compared. Therefore, the resistance between two stripe contacts was measured. The total resistance R_{tot} consists of the resistance of the contacts R_C and the semiconductor layer sheet resistance R_{Sh}, i.e. $R_{Sh} = R_{tot} - 2R_C$. The contact resistance was obtained from a fit of a series of stripe contacts with varying separation according to the transmission line model [16]. For the calculation of the sheet resistance of the layer, its thickness of 600 nm, the distance between the stripes and the width of the layer (=width of the stripes) were taken into account. Thereby, mobilities of 14.3 ± 0.7 and $4.2 \pm 0.5\,cm^2\,V^{-1}\,s^{-1}$ were derived for samples (d) and (e), respectively. These values are only slightly lower than those obtained for ZnSe and ZnTe grown by MBE [17–19], demonstrating the potential for applications, e.g. as contact layers for ZnMgCdSeTe-based light emitters on InP.

5. Conclusions

Epitaxial growth and phosphorus doping of ZnSeTe layers on InP are demonstrated. A linear increase of the Te fraction in the solid phase is found for a linear reduction of the Se supply. The improvement of crystalline quality due to lattice match is demonstrated by X-ray $\omega/2\theta$ FWHM below 150 arcsec for 300 nm thick layers. Phosphorus doping leads to p-type conduction for a Te fraction above 46%. For $ZnSe_{0.5}Te_{0.5}$:P, a maximum free hole concentration of $1 \times 10^{17}\,cm^{-3}$ with a hole mobility of $14.3\,cm^2\,V^{-1}\,s^{-1}$ is found. Strained $ZnSe_{0.25}Te_{0.75}$:P with a free hole concentration of $3 \times 10^{18}\,cm^{-3}$ and a mobility of $4.2\,cm^2\,V^{-1}\,s^{-1}$ has been obtained.

References

[1] D.J. Chadi, Appl. Phys. Lett. 59 (1993) 3589.
[2] A. Kamata, H. Mitsuhashi, H. Fujita, Jpn. J. Appl. Phys. 35 (1996) L87.
[3] W.S. Kuhn, Dissertation, Univ. Regensburg, 1992.
[4] W. Lin, B.X. Yang, S.P. Guo, A. Elmoumni, F. Fernandez, M.C. Tamargo, Appl. Phys. Lett. 75 (1999) 2608.
[5] E. Preuss, B. Krahl-Urban, R. Buntz, Laue Atlas, Bertelsmann Universitätsverlag, Düsseldorf, 1974.
[6] B.J. Skinner, P.B. Barton Jr., Am. Mineral. 45 (1960) 612.
[7] H. Stanzl, Dissertation, Univ. Regensburg, 1995.
[8] N. Lovergine, M. Longo, P. Prete, C. Gerardi, L. Calcagnile, R. Cingolani, A.M. Mancini, J. Appl. Phys. 81 (1998) 685.
[9] M. Strassburg, M. Strassburg, O. Schulz, U.W. Pohl, D. Bimberg, D. Litvinov, D. Gerthsen, M. Schmidtbauer, P. Schaefer, J. Crystal Growth 221 (2000) 416.
[10] S. Nakashima, T. Fukumoto, A. Mitsuishi, J. Phys. Soc. Jpn. 30 (1971) 1508.
[11] K. Wolf, H. Stanzl, A. Naumov, H. Wagner, W. Kuhn, B. Hahn, W. Gebhardt, J. Crystal Growth 138 (1994) 412.

[12] D.J. Dunstan, J.E. Nicholls, B.C. Cavanett, J.J. Davies, J. Phys. C 13 (1980) 6409.
[13] I.S. Hauksson, J. Simpson, S.Y. Wang, K.A. Prior, B.C. Cavenett, Appl. Phys. Lett. 61 (1992) 2208.
[14] R. Baltramiejunas, V.D. Ryzhikov, V. Gavryushin, A. Kazlauskas, G. Raciukaitis, V.I. Silin, D. Juoddzbalis, V. Stepankevicius, J. Lumin. 52 (1992) 71.
[15] G. Neu, E. Tournié, C. Morhain, M. Teisseire, J.-P. Faurie, Phys. Rev. B 61 (2000) 15789.
[16] H.H. Berger, Solid State Electron. 15 (1972) 145.
[17] T. Matsuoka, A. Ohki, T. Ohno, Y. Kawaguchi, J. Crystal Growth 138 (1994) 727.
[18] I.W. Tao, M. Jurkovic, W.I. Wang, Appl. Phys. Lett. 64 (1994) 1848.
[19] S. Nakatsuka, J. Gotoh, K. Mochizuki, A. Taike, M. Kawata, M. Momose, Jpn. J. Appl. Phys. 35 (1996) 1431.